Coupling Continuum to Molecular Dynamics Simulation: Feedback Control Formalism and Implementation

Dongyi Liao, Ju Li, Sidney Yip
Department of Nuclear Engineering
Massachusetts Institute of Technology, Cambridge, MA 02139

In this the second of a two-part paper we formulate a method for coupling atomistic and continuum simulations in the framework of the classical alternating Schwarz method with domain decomposition. Our approach combines the previously developed thermodynamic field estimator, which acts to extract the macroscopic field from the results of atomistic simulation, with a novel procedure, optimal in the sense of least disturbance, for imposing prescribed continuum boundary conditions on the atomistic system. By means of simple feedback control, we further ensure that the desired macroscopic field is achieved at the physical boundary by adjusting the imposed field at an extended boundary. Validity of our method is demonstrated in the example of simple Couette flow where the continuum solution is known analytically.

PACS number: 02.70.Ns, 47.11.+j, 83.10.Pp

I. INTRODUCTION

Molecular dynamics (MD) plays a unique role in the simulation of fluids by virtue of its ability to offer insights into atomic-level structure and dynamics that cannot be obtained from continuum calculations. Because only a microscopic region of the fluid can be studied in this manner, there is considerable interest to develop hybrid atomistic-continuum methods. The central issue here is the coupling, or matching, of discrete particles with continuum representation of the system, whose degrees of freedom are very different although physically related. Though this problem has been well recognized[1], there still appears to be no completely satisfactory solution.

Two notable attempts have been made recently to rectify this situation, both invoking the use of an overlapping region but differing in how the molecular and continuum descriptions are to be made compatible. O'Connell and Thompson[2] proposed to constrain the dynamics of atoms in the hybrid layer between the MD and continuum regions to ensure continuity of property averages across the coupling region. Hadjiconstantantinou and Patera[3] cast their formulation in the framework of alternating Schwarz method[5,6] and treated the matching in terms of refining the boundary conditions imposed on each of the overlapping subdomains through an iterative process.

In this paper we present a formalism for hybrid atomistic-continuum simulation, also in the spirit of the alternating Schwarz method, and focus on the problem of coupling continuum solution, in the form of phase space distribution (fields), to a system of discrete particles. The essence of the Schwarz method is to solve for the two overlapping subdomains in an iterative fashion (see Fig. 10), first obtaining the solution in one subdomain using an approximate boundary condition inside the other subdomain, then doing the same for the other subdomain based on the newly obtained solution, and iterating on

this sequence of steps until convergence is reached.

In this work the atomistic subdomain will be treated by MD simulation, while the other subdomain will be treated by an appropriate continuum solver. Coupling the two means that the boundary condition for the atomistic region will have a part determined by the continuum solution (on the border joining the overlapping region and the continuum), and vice versa. In order to iterate between continuum and MD solutions, one needs methods to carry out two types of operations, one is to construct the macroscopic field(s) that accurately represents a given set of particle data, and the other is to perform the inverse, which is to make sure that the MD particle trajectories correspond to a prescribed macroscopic field, and is achieved with as little artificial disturbance as possible. A method for the former has been developed in our first paper[4] in the form of an algorithm called the Thermodynamic Field Estimator (TFE). A method for latter operation is what we will describe below, to be named the Optimal Particle Controller (OPC).

The basis of OPC is a transformation relating two sets of random variables, each governed by a distribution function with certain macroscopic fields serving as parameters. In conjunction with TFE, this transformation allows us to impose arbitrary continuum solution as boundary condition for MD simulation. We regard this particular coupling procedure as optimal in the sense that the resulting artificial disturbance to the particle dynamics, as measured in terms of the square deviation in the two sets of random variables, is minimal.

Our coupling method incorporates another technique, designed to reduce further the artificial disturbance of imposing a prescribed macroscopic field. This involves applying the boundary condition at a distance extended beyond the MD-continuum interface normally associated with Schwarz-type overlapping domain decompositions. Using a first-order feedback control algorithm relating the field actually imposed at the extended boundary and the intended field at the MD-continuum interface, we show that faster convergence to the prescribed field can be achieved. We will refer to this procedure as the Extended Boundary Condition (EBC).

To demonstrate the validity of our hybrid atomistic-continuum simulation formalism, with emphasis on the atomistic aspects, we consider a particularly simple problem, that of planar Couette flow between two parallel walls. In this case the continuum solution is simply a linear flow velocity field, which conveniently eliminates the need for a real continuum solver, but suffices to illustrate the ideas.

This paper is organized as follows. We begin with the development of the Optimal Particle Controller in Sec.II, first defining a simple measure of disturbance to the particle dynamics, then formulating the optimal transformation, and lastly deriving the various distributions needed for the implementation. Given the OPC as a direct method of imposing field boundary condition on a system of particles with least disturbance, one can proceed in an

even more gentle manner by incorporating the Extended Boundary Condition and feedback control, discussed in Sec.III. Validation of our method which involves all three techniques, TFE, OPC, and EBC, in the case of Couette flow, is first discussed without reference to the larger picture of alternating Schwarz method, in Sec.IV. And then in Sec.V we consider specifically the effects of different types of Schwarz iterations on the convergence of the solution. A number of concluding remarks are offered in Sec.VI.

II. OPTIMAL PARTICLE CONTROLLER

A. Minimal Disturbance to Particle Dynamics

The basic problem we face is the following. Given a set of particle coordinates in phase space, namely the positions and velocities of a system of N particles, which can be reasonably well described by a distribution function characterized by a set of macroscopic fields (density, velocity, and temperature)[4]. How does one modify the particle coordinates such that the corresponding distribution is now characterized by a different set of macroscopic fields? Stated in another way, given that the current particle coordinates are governed by a certain distribution function, how does one find a new set of coordinates which are governed by a different distribution, the one that is prescribed by the continuum subdomain solution? One may try to decouple the two first, and use only the latter to sample the new set of coordinates. While this would indeed lead to a coupling scheme, it is quite conceivable that ignoring the current state will result in a procedure which strongly disturbs the particle dynamics. If decoupling the two distributions, or equivalently, the two sets of particle coordinates, is not a good idea, then one should look for a way to relate them such that the disturbance is minimized. We will now introduce a quantitative measure of this disturbance and suggest a relation connecting the current state and the desired state that minimizes this measure.

To be explicit we consider a coupling scheme where the continuum velocity field is imposed on the atomistic simulation, and for the moment suppose we already know the transformation that are to give the desired continuum field. Then we can define

$$B = \sum_n |\Delta \mathbf{v}_n|^2 = \sum_n |\mathbf{v}_n^{\text{out}} - \mathbf{v}_n^{\text{in}}|^2, \tag{2.1}$$

where $\Delta \mathbf{v}_n$ is the change in particle velocity of the nth particle ($\mathbf{v}_n^{\text{in}}$ and $\mathbf{v}_n^{\text{out}}$ are the velocity before and after the transformation). This quantity will be used as a simple measure of the artificial disturbance to particle dynamics, which should be minimized as much as possible.

For the developments to follow, we note that a reasonable form to take for the distribution which describes the particle coordinates is the local Maxwellian function

$$dP = f_M\left(\mathbf{x},\mathbf{v}|\{\rho(\mathbf{x}),T(\mathbf{x}),\bar{\mathbf{v}}(\mathbf{x}\}\right)d\mathbf{x}d\mathbf{v} \qquad (2.2)$$
$$= \rho(\mathbf{x})d\mathbf{x}\cdot\frac{1}{(2\pi T(\mathbf{x}))^{D/2}}\exp\left(-\frac{|\mathbf{v}-\bar{\mathbf{v}}(\mathbf{x})|^2}{2T(\mathbf{x})}\right)d\mathbf{v},$$

where $\mathbf{x}$, $\mathbf{v}$ are single particle position and velocity, and $\rho(\mathbf{x})$, $T(\mathbf{x})$, $\bar{\mathbf{v}}(\mathbf{x})$ are the macroscopic density, velocity and temperature fields, respectively. In (2.2) D is the dimensionality of the system, and we have taken the mass of particles and the Boltzmann constant to be unity.

Consider now the different ways one can modify the existent particle velocities to achieve a distribution that is characterized by a different macroscopic field. We can think of two criteria which need to be satisfied. First, the resulting macroscopic field must be correct. A common way to estimate the macroscopic field from particle data is to assume a distribution and calculate its averaged moments. In most situations a local Maxwellian form (2.2) provides a good description, and that can always be explicitly checked. Second, correct particle dynamics is desired. If the particle dynamics is strongly disturbed, MD simulation will lose its physical significance. Conforming to a prescribed distribution does not mean that the dynamics is also correct. If a macroscopic field has reached the correct value and can be maintained without further coupling, a good controller should do nothing more to the particles. This means that the modified phase coordinates should not be decoupled from the original ones.

As an illustration let us consider a simple problem of 1D convection-less heat conduction, for which we wish to impose a temperature boundary condition of high temperature T_h on the left ($x = 0$) and low temperature T_l on the right ($x = 1$). Intuitively one could imagine doing the following.

When a particle crosses either boundary ($x = 1$ or $x = 0$), give it a random velocity drawn from distribution (2.2) with parameters $\bar{\mathbf{v}} = 0$ and $T = T_h$ (or $T = T_l$). However, this procedure can be shown not to work. When implemented in practice, the case of homogeneous heating ($T_h = T_l$) shows that the bulk temperature reaches a value of $T_h/2$.

The above scheme fails because one is dealing with a conditional probability problem. The speed distribution of atoms which cross the boundary is *different* from the speed distribution of atoms in the bulk

$$dP = \frac{1}{\sqrt{2\pi T}}\exp\left(-\frac{v^2}{2T}\right)dv, \qquad -\infty < v < +\infty \quad (2.3)$$

Instead it is weighted by the normal velocity,

$$dP = \frac{v\exp\left(-\frac{v^2}{2T}\right)dv}{\int_0^{+\infty} v\exp\left(-\frac{v^2}{2T}\right)dv}$$
$$= \frac{v}{T}\exp\left(-\frac{v^2}{2T}\right)dv, \qquad 0 < v < +\infty. \qquad (2.4)$$

$\langle v^2\rangle$ from distribution (2.4) is $2T$, not T. Thus, if we sample the *boundary crossing atoms* using bulk distribution (2.3) with parameter $T = T_h = T_l$, the energy can

only be balanced (in a statistical sense) when the bulk temperature reaches $T_h/2$.

A more subtle defect of this scheme is that, for whatever the incoming velocity $v_{\rm in}$ of the particle before hitting the boundary, a new velocity $v_{\rm out}$ is drawn from a given distribution, say $g(v)$, entirely *independent* of $v_{\rm in}$. Thus if we evaluate the disturbance to particle dynamics using (2.1), it is always substantial no matter how long one runs the simulation. In the example of homogeneous heating, where the correct distribution (2.4) is used as $g(v)$ in drawing $v_{\rm out}$'s, even when the system reaches the desired temperature, the scheme continues to disturb the particles by giving each boundary crossing atom a new $v_{\rm out}$. On the other hand, if we just let $v_{\rm out} = v_{\rm in}$, i.e., do nothing, the system temperature stays at T_h! A more intelligent particle controller should automatically tune down its influence as the system approaches the desired state, a behavior we may call the coalescence property.

B. The Optimal Transformation

We now formulate the above considerations mathematically. Suppose we have an incoming random variable series $\{X_n\}$, conforming to distribution function $f(X)$:

$$dP(\eta < X < \eta + d\eta) = f(\eta)d\eta, \tag{2.5}$$

and we would like the series to conform to a different distribution g. We propose to achieve this by replacing every X with another variable Y which is distributed according to g. Thus the goal is to find a transformation $\mathcal{T}$,

$$\mathcal{T} : X_n \to Y_n, \tag{2.6}$$

with the requirement that if $\{X_n\}$ conforms to distribution $f(X)$, $\{Y_n\}$ will conform to distribution $g(Y)$:

$$dP(\xi < Y < \xi + d\xi) = g(\xi)d\xi. \tag{2.7}$$

There are many possible $\mathcal{T}$'s. However our previous discussion shows that the following property is desirable: *if $f \equiv g$, then $\mathcal{T}$ gives $Y_n \equiv X_n$.*

To incorporate the idea of *minimally disturbing the dynamics*, we adopt the criterion that

$$B[\mathcal{T}] = \langle (Y - X)^2 \rangle \tag{2.8}$$

be minimized among all possible $\mathcal{T}$'s.

Thus our output series $\{Y_n\}$ is least altered from $\{X_n\}$, while it is still distributed according to $g(Y)$. As f approaches g, Y approaches X.

We see that if $\mathcal{T}$ is randomly drawing Y from $g(Y)$ without reference to X, it satisfies the basic requirement of (2.7) but not the coalescence property. We will call this transformation $\mathcal{T}_1$.

To incorporate coalescence one may consider the transformation $\mathcal{T}_2$,

$$\mathcal{T}_2 : \begin{cases} Y = X : & p \leq \frac{g(X)}{Kf(X)} \\ \\ \text{draw } Y \text{ randomly from } g(Y) : & p > \frac{g(X)}{Kf(X)} \end{cases}$$

where p is a random number uniformly distributed over $[0, 1]$, and K is a constant (scheme fails if K does not exist) such that

$$Kf(X) \geq g(X) \text{ for } -\infty < X < +\infty. \tag{2.9}$$

But is $\mathcal{T}_2$ the best one?

We propose the following transformation, in the form of an implicit relation,

$$\mathcal{T}_3 : X \to Y \sim \int_{-\infty}^{X} f(\xi)d\xi = \int_{-\infty}^{Y} g(\xi)d\xi. \tag{2.10}$$

It can be checked that Y indeed conforms to distribution $g(Y)$ if the incoming random number X conforms to distribution $f(X)$, and it satisfies the coalescence property. In fact this should come as no surprise because it is the only one-to-one continuous mapping which satisfies (2.7), without the extra randomness like in $\mathcal{T}_2$.

We believe that $\mathcal{T}_3$ is the mathematically optimal transformation which minimizes (2.8). A plausibility argument is given in the Appendix. Our experience has shown that while $\mathcal{T}_3$ works rather well, it is an implicit algorithm and could be computationally demanding.

Thus far we have assumed $f(X)$ to be known. In reality it has to be inferred from $\{X_n\}$, and this invokes the separate issue of how we extract continuum representation from the atomistic description. A straightforward approach would be to collect $\{X_n\}$ over a period of time to compile a histograph. For fields with spatial and temporal variations this is not a very good idea, especially if the available data set is small. If one believes that the *actual* field has smooth variation, then particle data outside the point of interest carry useful information about the field at this point and should not be discarded. One then should use the Thermodynamic Field Estimator introduced in the first paper[4]. The continuous representation given by this method is based on the principle of Maximum Likelihood Inference and a judicious choice of basis functions, which makes good use of all available information. It is assumed in this method as well, that the local-equilibrium distribution (2.2) holds, which is the bridge between macroscopic fields (continuum) and microscopic statistical mechanics (MD).

C. 3D Implementation

To implement the foregoing formulation we need to find the coupling distributions f and g that will relate the continuum description to an atomistic system. Since

the coupling takes place through the particle velocities, we will give in this section explicit expressions for the velocity distribution. With $D = 3$ and particles conforming to distribution (2.2) with microscopical fields $(\{T(\mathbf{x}), \bar{\mathbf{v}}(\mathbf{x})\})$, we calculate the boundary crossing rate at $\partial\mathcal{C}$ (see Fig. 1) for any small piece of the surface area. For choice of the coordinate system, we take the transverse basis $\mathbf{s}$ and $\mathbf{t}$ such that the macroscopic field $\bar{\mathbf{v}}(\mathbf{x})$ lies entirely in the place of $\mathbf{n}$ and $\mathbf{s}$. Thus, in this local frame,

$$\bar{\mathbf{v}} = (\bar{v}_n, \bar{v}_s, 0), \tag{2.11}$$

(from now on we will omit $\mathbf{x}$ but it is implicitly understood that everything is local). In the same frame the particle velocities can be expressed as

$$\mathbf{v} = (v_n, v_s, v_t). \tag{2.12}$$

The boundary crossing rate from interior to exterior is

$$\begin{aligned}
&\left.\frac{dN}{dSdt}\right|_{-\mathbf{n}\to\mathbf{n}} \\
&= \rho \int_{v_n>0} \exp\left(-\frac{(v_n-\bar{v}_n)^2+(v_s-\bar{v}_s)^2+v_t^2}{2T}\right) \frac{v_n dv_n dv_s dv_t}{(2\pi T)^{3/2}} \\
&= \frac{\rho}{\sqrt{2\pi T}} \int_0^{+\infty} v_n \exp\left(-\frac{(v_n-\bar{v}_n)^2}{2T}\right) dv_n \\
&= \frac{1}{2}\rho\bar{v}_n \left(1+\operatorname{erf}(\frac{\bar{v}_n}{\sqrt{2T}})\right) + \frac{\rho T}{\sqrt{2\pi T}} \exp(-\frac{\bar{v}_n^2}{2T}),
\end{aligned} \tag{2.13}$$

where the error function is defined as

$$\operatorname{erf}(x) = \frac{2}{\sqrt{\pi}} \int_0^x \mathrm{e}^{-\eta^2} d\eta.$$

Similarly the reverse crossing rate is

$$\begin{aligned}
&\left.\frac{dN}{dSdt}\right|_{\mathbf{n}\to-\mathbf{n}} \\
&= -\frac{1}{2}\rho\bar{v}_n(1+\operatorname{erf}(\frac{-\bar{v}_n}{\sqrt{2T}})) + \frac{\rho T}{\sqrt{2\pi T}} \exp(-\frac{\bar{v}_n^2}{2T}).
\end{aligned} \tag{2.14}$$

With the boundary crossing rate depending only on the normal component of the field velocity, the distribution function which relates the particle and field variables becomes three decoupled distributions. For the boundary hitting $(-\mathbf{n}\to\mathbf{n})$ atoms, they are

$$\begin{aligned}
&g_n(v_n) = \frac{(2\pi T)^{-1/2} v_n \exp(-(v_n-\bar{v}_n)^2/2T)}{\frac{1}{2}\bar{v}_n(1+\operatorname{erf}(\frac{\bar{v}_n}{\sqrt{2T}})) + \sqrt{\frac{T}{2\pi}}\exp(-\frac{v_n^2}{2T})} \\
&v_n \in (0, +\infty),
\end{aligned} \tag{2.15}$$

$$\begin{aligned}
&g_s(v_s) = \frac{1}{\sqrt{2\pi T}} \exp(-(v_s-\bar{v}_s)^2/2T) \\
&v_s \in (-\infty, +\infty),
\end{aligned} \tag{2.16}$$

$$\begin{aligned}
&g_t(v_t) = \frac{1}{\sqrt{2\pi T}} \exp(-v_t^2/2T) \\
&v_t \in (-\infty, +\infty).
\end{aligned} \tag{2.17}$$

Notice we use symbol g here to indicate that $(T, \bar{\mathbf{v}})$ are the *desired* macroscopic fields. In order to achieve these fields using $\mathcal{T}_3$ transformation (2.10) we need to know the f's, i.e., the *actual*, or current, velocity distribution functions of boundary hitting atoms. They are also given by (2.2) but with different parameters $(T', \bar{\mathbf{v}}')$. If we express

$$\bar{\mathbf{v}}' = (\bar{v}'_n, \bar{v}'_s, \bar{v}'_t) \tag{2.18}$$

in the same coordinate frame and repeat the steps (2.13) to (2.17), we get corresponding results for the distributions describing the current state,

$$f_n(v_n) = \frac{(2\pi T')^{-1/2} v_n \exp(-(v_n - \bar{v}'_n)^2/2T')}{\frac{1}{2}\bar{v}'_n(1 + \mathrm{erf}(\frac{\bar{v}'_n}{\sqrt{2T'}})) + \sqrt{\frac{T'}{2\pi}}\exp(-\frac{\bar{v}'^2_n}{2T'})}$$
$$v_n \in (0, +\infty), \tag{2.19}$$

$$f_s(v_s) = \frac{1}{\sqrt{2\pi T'}}\exp(-(v_s - \bar{v}'_s)^2/2T')$$
$$v_s \in (-\infty, +\infty), \tag{2.20}$$

$$f_t(v_t) = \frac{1}{\sqrt{2\pi T'}}\exp(-(v_t - \bar{v}'_t)^2/2T')$$
$$v_t \in (-\infty, +\infty). \tag{2.21}$$

Because the distributions in v_n, v_s, v_t are decoupled, we can apply (2.10) separately on the three variables, for each $-\mathbf{n} \to \mathbf{n}$ boundary hitting particle. The situation for $\mathbf{n} \to -\mathbf{n}$ is exactly the same after $v_n \to -v_n$ substitution.

All the above derivations for imposing boundary conditions do not include density coupling. To couple density, one has to inject or remove particles, then the disturbance to particle dynamics cannot be quantified by what we are proposing here. Maintaining certain density field is in general more difficult than maintaining temperature or velocity field. On the other hand, one usually are not required to apply density boundary condition explicitly. In most problems, the density field rather comes as a response to the other fields through the equation of state, for example in the micro-channel Poiseuille flow problem discussed in our first paper[4].

III. EXTENDED BOUNDARY CONDITION

In Section II a method was proposed to control the field boundary condition of an MD simulation which results in least disturbance to the particle dynamics in the sense of (2.1). Nevertheless the disturbance is still existent for particles in the skin region near the boundary, which can be shown to be proportional to the rate of dissipation in the system. In this Section we will formulate a procedure which eliminates that disturbance entirely at the specified boundary. Since any artificial action necessarily

alters the particle dynamics in the vicinity where it is imposed, the best one can do is to act some distance away from the intended boundary and cause the macroscopic field at the boundary to be what is prescribed.

This can be done using a three-region approach which we will call the *Extended Boundary Condition (EBC)*, shown in Fig. 2, and through a feedback control mechanism. The physical region of interest, $\mathcal{C}$ (core), is surrounded by a buffer zone $\mathcal{B}$. Actions are applied on an outer MD region $\mathcal{A}$ which is sufficiently separated from $\mathcal{C}$, its aim being to induce the prescribed field boundary conditions on the core boundary $\partial\mathcal{C}$. Due to molecular chaos in fluids, perturbation to particle dynamics will decay over a distance of a few mean free paths, thus setting a lower limit for $\mathcal{C}$-$\mathcal{A}$ separation. The action in $\mathcal{A}$ is in general a matter of choice, but here we will use the OPC developed in last section because it minimizes the disturbance, thus $\mathcal{B}$ could be as thin as possible. The TFE serves as the detector of the control loop, inferring current fields on $\partial\mathcal{C}$ based on particle data from the entire $\mathcal{C}$ region. A Control Algorithm compares the estimated current field with the prescribed field on $\partial\mathcal{C}$, and gives instructions to the particle controller.

Note that although $\mathcal{A}$ and $\mathcal{B}$ are discrete particle regions governed by the same molecular dynamics as $\mathcal{C}$, they are conceptual constructs which have no physical correspondence and do not appear explicitly anywhere in Fig. 10. They exist solely to ensure that the physical region of interest $\mathcal{C}$ has the correct field boundary conditions and evolves according to natural particle dynamics. Properly implemented, it could be a powerful tool for studying fluid systems because a fluid atom in $\mathcal{C}$ has no way to tell any difference from reality. It in turn can be used as a perfect benchmark for comparing the actual performance of $\mathcal{T}_1$ and $\mathcal{T}_3$, as we will see below.

We now demonstrate how such a procedure could be implemented in the context of simulation of shear flow. In classic Couette flow problem, the continuum fluid moves between parallel sliding plates with a linear velocity profile as shown in Fig. 3. The entire fluid is of macroscopic dimension ($> \mu$m). The part of the problem which is appropriate for MD simulation is only a small region at the fluid-wall interface. This atomistic region is depicted as consisting of three layers of atoms representing the wall and a fluid of N atoms. To maintain the flow field, a boundary action representing the continuum-atomistic coupling acts at plane $\partial\mathcal{A}$ in Fig. 4 which, as we saw, need not to be the outer boundary of the physical core (subdomain) $\partial\mathcal{C}$. But as a comparison, we will also implement the direct Particle Controller (PC) approach shown in Fig. 5, where $\partial\mathcal{A}$ *is* $\partial\mathcal{C}$ and there is no buffer zone.

In practice it is more convenient to work with a simulation cell that is periodic in the z-direction, for this reason our MD simulation will be carried out in a symmetric geometry as shown in Fig. 4 and 5. Since our MD program is $\mathcal{O}(N)^4$, this merely doubles the computational effort but we get twice as much particle data as well; and with each side serving as a particle reservoir for

the other. It is important to keep in mind the connection between this particular simulation setup and the Couette flow problem in the framework of Schwarz coupling (Fig. 10); otherwise, the significance of simulating a periodic system of fluids flowing between static walls driven by a velocity field along the center line may not be apparent.

In applying the EBC (Fig. 4), the buffer region is between $\partial\mathcal{A}$ and $\partial\mathcal{C}$. Actions are applied on $\partial\mathcal{A}$ instead of $\partial\mathcal{C}$ in such a way that the desired field at $\partial\mathcal{C}$ is obtained (see Fig. 4). The question then becomes, given the desired flow velocity at $\partial\mathcal{C}$, v_C^*, how does one control the flow velocity at $\partial\mathcal{A}$ (prescribed value of the OPC), v_A^*? Adopting a first-order feedback control algorithm, we may write

$$\frac{dv_A^*(t)}{dt} = -\kappa(v_C(t) - v_C^*), \tag{3.1}$$

where the rate constant κ should be picked according to the response time at $\partial\mathcal{C}$ due to an action on $\partial\mathcal{A}$, to make (3.1) converge as quickly as possible without oscillations[7]. This simple equation allows us to control the action on $\partial\mathcal{A}$ based on current values at $\partial\mathcal{C}$ and $\partial\mathcal{A}$ (from TFE), as well as prescribed value at $\partial\mathcal{C}$.

A further drawback of the direct approach (Fig. 5) besides disturbing the particle dynamics is that in a system with finite dissipation, we have to "overshoot" in the prescribed field value by some unknown amount in order to achieve the desired value at the same locale, because dissipation is always dragging the gradients down, and the particle controller only acts when the current value is off, so the time-averaged value is always below what is prescribed. The problem is, we do not know beforehand how much overshooting is needed to achieve the desired field. If the dissipation is zero (as in the homogeneous heating case), then we do not need overshooting at all and the coalescence property works perfectly. But in case of finite dissipation, its influence on the results of direct PC approach is significant (see Fig. 7 in the following section). This problem can only be satisfactorily handled by the EBC, where the feedback control mechanism automatically takes care of the overshooting, and not on $\partial\mathcal{C}$ but $\partial\mathcal{A}$.

IV. COUETTE FLOW TEST

In this Section we demonstrate how the above ideas are implemented for Couette flow. The process is somewhat reversed: we first implement the direct approaches (Fig. 5) using $\mathcal{T}_1$ and OPC, obtain the actual flow velocity value at $\partial\mathcal{C}$ which has dropped somewhat from the prescribed value due to dissipation, and use EBC to reproduce that actual value at $\partial\mathcal{C}$ by acting on $\partial\mathcal{A}$ (Fig. 4). We then in turn calculate a specially defined particle velocity auto-correlation function with EBC, and compare with those of the direct approaches, to show that OPC is indeed much more effective than $\mathcal{T}_1$ in preserving the particle dynamics.

Consider a fluid of atoms which interact through a Lennard-Jones 6-12 interatomic potential with a cutoff at $r_c = 2.2\sigma$,

$$V = \begin{cases} 4\varepsilon \left[(\frac{\sigma}{r})^{12} - (\frac{\sigma}{r})^6 - (\frac{\sigma}{r_c})^{12} + (\frac{\sigma}{r_c})^6 \right] & (r < r_c) \\ 0 & (r \geq r_c). \end{cases}$$

The interaction parameters define a set of reduced units: length in terms of σ, energy in terms of ε, mass in terms of single fluid particle mass m. Thus one reduced time unit is $\tau = (m\sigma^2/\varepsilon)^{1/2}$, one reduced velocity unit is $(\varepsilon/m)^{1/2}$, etc. All numbers given in this paper are in reduced units unless otherwise specified.

The wall consists of three layers of atoms fixed in fcc structure which interact with the fluid atoms also through a Lennard-Jones 6-12 potential but with parameters $\varepsilon_{wf} = 2\varepsilon$ and $\sigma_{wf} = \sigma$. This choice of parameters gives a more pronounced nonlinear effect near the fluid-wall interface.

The core region $\mathcal{C}$ has size $(L_x, L_y, L_z) = (8, 8, 10)$, with the wall occupying 20% and the fluids 80%. The buffer zone $\mathcal{B}$ has size $(8, 8, 1)$. The action region $\mathcal{A}$ is just a plane $\partial\mathcal{A}$ here, meaning that we only act on particles passing through the plane. As mentioned above, the real simulation cell contains two identical, mirror-reflected systems, so the size of simulation cell is $(8, 8, 22)$ for EBC simulations (Fig. 4) and $(8, 8, 20)$ for direct PC simulations (Fig. 5); the total number of particles is $N = 979$ and 870, respectively. For the fluid state, we choose density $\rho = 0.81$ and temperature $T = 1.2$ to ensure that it is in stable liquid phase.

As a check of the simulations, we plotted in Fig. 6 the fluid density profile across the simulation cell with and without an imposed velocity field the centerline. One sees the familiar layering effect near the wall[8]; apparently the presence of a flow field has no discernible effect on the density profile.

Fig. 7 shows the profile of shear flow velocity with distance normal to the fluid-wall interface, which starts at the interface ($z = 2$) and extends into the bulk. A continuum field boundary condition $v_x = 0.12$ is to be achieved on the $\partial\mathcal{C}$ plane. Three sets of simulation results are shown. Two (stars and circles) are obtained by directly applying the particle controllers $\mathcal{T}_1$ and OPC on plane $\partial\mathcal{C}$ (Fig. 5), with prescribed velocity value $v_x = 0.2$ ("overshooting") to counteract the dissipation. The third (solid line) result is obtained by using the EBC (Fig. 4) to achieve $v_x = 1.2$ on $\partial\mathcal{C}$, and serves as the benchmark of this test. It can be seen that overall, all three results agree well away from the artificial action region, with linear velocity profile in the bulk and strongly nonlinear behavior near the fluid-wall interface. However, the direct approaches have no way to determine the amount of overshooting *a priori*; and the deleterious effects of sudden velocity drop near the action zone boundary due to dissipation, and the artificial disturbance to particle dynamics, are completely avoided in the EBC simulation for $\partial\mathcal{C}$, to be replaced by what is happening near $\partial\mathcal{A}$.

To show how the feedback control mechanism works, we start with a stationary fluid, and let the desired boundary condition at $\partial\mathcal{C}$ to be $v_C^* = 0.12$. Starting with $v_A^*(0) = 0.12$, Fig. 8 shows how $v_A^*(t)$ evolves according to (3.1), and how $v_C(t)$ responds to that action on $\partial\mathcal{A}$, separated by a buffer. A rate constant of $\kappa = 0.024$ is picked for the current buffer thickness of 1. To filter out the large thermal noises residing in instantaneous $v_C(t)$, it is plotted in Fig. 8 after a sliding bin average of $\Delta t = 50$. We can see that $v_C(t)$ converges to the desired value of $v_C^* = 0.12$ at about $t = 80$, while $v_A^*(t)$ has also converged to a value of about 0.21.

To quantify the effectiveness of OPC in preserving the particle dynamics, let us consider a quantity which represents the microscopic dynamics much better than the overall flow velocity. The velocity autocorrelation function is a quantity in the theory of liquids which is an important characteristic of single-particle motion. We can define its localized and normalized version

$$\Psi(t) = \frac{\langle \mathbf{v}_i(0) \cdot \mathbf{v}_i(t) \rangle}{\langle \mathbf{v}_i(0)^2 \rangle}, \tag{4.1}$$

for any ith particle which crosses the $\partial\mathcal{C}$ plane and comes into $\mathcal{C}$ region at a certain moment; its contribution to $\Psi(t)$ is terminated whenever the particle re-crosses that plane. Since the EBC acts on $\partial\mathcal{A}$ instead of $\partial\mathcal{C}$, $\Psi_{\rm EBC}(t)$ should be the same as that of nature where no artificial disturbance is discernible locally. On the other hand, it is not so if we directly act on $\partial\mathcal{C}$. However, $\Psi(t)$ of OPC direct should be better than that of $\mathcal{T}_1$ direct in comparing with $\Psi_{\rm EBC}(t)$. Fig. 9 shows the difference $\Psi_{\rm EBC}(t) - \Psi_{\mathcal{T}_1}(t)$ in stars and $\Psi_{\rm EBC}(t) - \Psi_{\rm OPC}(t)$ in circles; the three functions themselves are plotted in the upper right inset. Notice that $\Psi_{\mathcal{T}_1}(t = 0)$ is 1 as expected, but there is a drastic loss of correlation in the first $0.05ps$, clearly attributable to the drastic reaction of surrounding atoms when its direction is suddenly altered without considering its original motion. On the other hand, $\Psi_{\rm OPC}(t)$ is almost indistinguishable from $\Psi_{\rm EBC}(t)$. This is reasonable since $\Psi(t)$ is normalized, and the shear flow velocity is only a fraction of the particle total velocity.

V. THE SCHWARZ COUPLING METHOD

Hadjiconstantinou and Patera[3] have proposed to couple atomistic and continuum simulations of fluid flow based on a classical procedure known as domain decomposition and the alternating Schwarz method[5,6]. In this approach one divides the domain into two or more overlapping subdomains and treats each one separately through an iterative procedure where the boundary conditions for one subdomain are derived from the solutions for the other subdomains. Suppose our domain of interest is decomposed into two subdomains $\mathcal{C}$ and $\mathcal{U}$, with an overlapping region bounded by two boundaries, $\partial\mathcal{C}$ and $\partial\mathcal{U}$, as shown in Fig. 10. To obtain the solution for

the entire domain, one iterates on the following. Starting with a trial boundary condition on $\partial\mathcal{C}$ which we denote as v_C^0, one obtains the solution for the subdomain $\mathcal{C}$. With this initial solution one then determines what is the boundary condition on $\partial\mathcal{U}$, denoted as v_U^1. Knowing this, one obtains the solution in subdomain $\mathcal{U}$. Now a refined value for the boundary condition on $\partial\mathcal{C}$, v_C^1, can be determined to go on with the next iteration. The alternating process continues until convergence is reached in both subdomains. For a large class of problems where both subdomains are treated by continuum solvers, convergence can be proved[6]. When one of the subdomains is treated atomistically, convergence should be similarly achieved so long as the overlapping region is describable by both continuum and atomistic representations.

To implement the alternating Schwarz method in our simulation of shear flow we consider the system is decomposed into two overlapping regions (Fig. 11), with $\mathcal{C}$ being the atomistic region, $\mathcal{U}$ the continuum, and an overlapping region bounded by planes $\partial\mathcal{C}$ and $\partial\mathcal{U}$. In the event that the computational costs involved in determining the velocity fields in the two regions are markedly different, we have found (see below) it is more efficient not to wait for the slow solver to converge, since the initial boundary conditions for the subdomains are not likely to be accurate. With the present continuum region always characterized by a linear velocity field, the calculation required for the continuum part of the iteration is just a linear interpolation. Given the current or averaged velocity field at plane $\partial\mathcal{U}$, the desired boundary value at plane $\partial\mathcal{C}$ is readily obtained as

$$v_C^* = \frac{(d_{CU} v_Z + d_{ZC} v_U)}{d_{ZU}}, \tag{5.1}$$

where v_Z is a constant which sets the magnitude of the velocity on the real boundary $\partial\mathcal{Z}$ of continuum region (see Fig. 11), d_{CU} is the distance between $\partial\mathcal{C}$ and $\partial\mathcal{U}$, etc. In the following simulations, the values are $v_Z = 0.2$, $d_{CU} = 3$, $d_{ZC} = 8$ and $d_{ZU} = 11$ (in a real simulation d_{ZU} should be much larger). Taking advantage of the fact that the the continuum solver requires no computational effort, we update the boundary condition at plane $\partial\mathcal{C}$ after every MD step. This is tantamount to relaxing both boundary conditions simultaneously. The MD solver is realized using EBC and (3.1) developed in section III.

Fig. 12 shows the convergence of shear flow velocities at plane $\partial\mathcal{C}$ to the value given by the continuum solution. The fluid atoms are given initial velocities sampled from (2.2) according to a uniform temperature field and a linear velocity field. At beginning of the simulation the desired velocity at plane $\partial\mathcal{C}$ is set to a value of 0.1 based on the above initial guess. A simulation is taken following the classical alternating Schwarz method, where at each iteration the MD calculation is carried out to convergence. At this point the flow velocity at $\partial\mathcal{U}$ is averaged for previous $500,000$ timesteps or 2500τ. This average v_U is used in (5.1) to update the desired value at plane

$\partial\mathcal{C}$, for the next period of MD simulation. The resultant v_C^* is shown in Fig. 12 in straight solid line.

One could also proceed in a slightly different manner, that is to adjust v_C^* using (5.1) after every MD step, as the continuum solution costs nothing here. The resultant v_C^* is shown in Fig. 12 as the zigzag solid line, after a sliding bin average of $\pm 1250\tau$. Convergence is achieved after a coupling time of 5000τ. One can see that the classical alternating Schwarz coupling may have a slower convergence here, by a factor of about 2, compared to the method of simultaneous relaxation at each MD step. Thus, invoking the two subdomain solvers in an asymmetrical fashion (one always converges, the other very little) leads to a more efficient scheme.

The fully converged, uniform hybrid continuum-atomistic solution is plotted in Fig. 13, for both the classical alternating Schwarz coupling (circles) and the new simultaneous coupling (stars). One should note the perfect matching between MD and continuum solution in the overlapping region.

In general, if the continuum solver also requires finite amount of computational effort, the continuum to MD coupling can be updated at intervals of n MD steps, with adjustable n. If $n = 1$, it is the simultaneous relaxation method; if n is a large number such that the MD solver fully converges each time, we recover the classical alternating Schwarz method. An optimal n can be chosen according to the ratio of computational costs of the two solvers in achieving respective convergence. Also notice that one needs to take care of the thermal noises coming out of the MD solution, although it may have been reduced somewhat by the TFE. In general, even if the continuum solver is very fast, one may still need to wait for a while for the MD solver to average out the thermal noises. Feeding large fluctuations into the continuum solver may likely cause oscillatory behavior or divergence. In our case, the continuum solver is linear and does not have a convergence problem, because the fluctuations which come into the continuum solver will go back linearly and be filtered out by feedback loop.

VI. DISCUSSIONS

We have developed a hybrid continuum-atomistic simulation scheme based on the concept of domain decomposition, in the same spirit as Hadjiconstantinou and Patera. Such methods are useful for problems where much of the region of interest can be treated by continuum description, but a small critical, embedded part requires atomistic simulation. While Hadjiconstantinou and Patera implemented their method with attention to both the atomistic and continuum representations, we have focused our efforts on techniques for coupling continuum boundary conditions to atomistic simulations. In this work matching of the two different levels of representation, each with its own set of degrees of freedoms, takes

place in the overlap region through an implicit transformation which we have called the Optimal Particle Controller, with the local Maxwellian distribution serving as the bridge, which depends on both particle and field variables. Relative to the conventional method of sampling from a desired distribution, such as the $\mathcal{T}_1$ transformation, OPC has the advantage that it is least disturbing to the particle dynamics, and that disturbance is proportional to the rate of dissipation, i.e., field gradients in the system instead of the absolute magnitude of the fields.

We have incorporated OPC along with the Thermodynamic Field Estimator and the Extended Boundary Condition into the framework of alternating Schwarz method and implemented our formalism in a study of shear flow. We should regard the numerical results presented here as proof of principle of the entire hybrid scheme. Since each one of these three techniques has its own novel features, further applications, including separate investigations of each technique, will be worthwhile to bring out their capabilities and limitations. We believe that relative to the other hybrid methods recently proposed[2,3] our method should be the most gentle as far as treating the atomistic subdomain is concerned. For this reason the method should be most useful when one is interested in delicate or subtle molecular effects where minimizing local disturbance to particle dynamics is a significant concern.

Up to now we have only concerned with ourselves steady state fluid problems. One may wonder if a continuum solver could be dynamically coupled with an MD solver using the above techniques in real time. We do not have the solution yet but it seems quite difficult. On the other hand, the timescale of an macroscopic dynamical event is usually much greater than that of its underlying microscopic mechanism, thus to the critical microscopic region at any given moment of the event, the outside would seem to be in a steady state flow condition and could be modeled by our techniques. Such is in fact the rationale behind constitutive equations; but it should be able to handle more complex databases as well, such as stick-slip motion and chemisorption.

The case for solids is different. Solids, unlike fluids, have long range order. The assumption of molecular chaos is invalid here, and a buffer zone cannot cover up the disturbed dynamics elsewhere, which is the underpinning of the Extended Boundary Condition. Thus, it is quite difficult to isolate a region in a crystalline material since the phonons have very long mean free paths, and their scattering and reflections determine important macroscopic properties such as the thermal conductivity. Although researchers have developed successful techniques to couple continuum with atomistic regions for static calculations[9], no one has yet claimed to successfully implement such a scheme to study finite temperature properties.

ACKNOWLEDGMENTS

This work was supported by a grant from the Sandia National Laboratory. We express our appreciation to C.-N. Wong for suggesting this problem as well as interest and support throughout its development. We also acknowledge helpful discussions with N. Hadjiconstantinou and A. Patera.

APPENDIX A: PROOF THAT $\mathcal{T}_3$ IS OPTIMAL

By our definition, a transformation is an operation which gives an output Y from an input X, but not necessarily in a deterministic manner, which differs from the concept of a function. $\mathcal{T}_1, \mathcal{T}_2$ and $\mathcal{T}_3$ in section (II B) are all examples of such transformations. Mathematically it is equivalent to a mapping from a real number $x = X$ to a real *function* in y, which is the conditional probability distribution $W(y|x)$, from which Y is drawn. The joint probability distribution function is simply

$$W(x, y) = W(y|x)f(x) \tag{A1}$$

for the two random variables on xy plane.

$W(x, y)$ has the properties of:

1. Non-negativeness:

$$\forall x, y \in (-\infty, +\infty) \quad W(x, y) \geq 0 \tag{A2}$$

2. Normalization:

$$\int_{-\infty}^{+\infty} W(x, y)dy = f(x) \tag{A3}$$

$$\int_{-\infty}^{+\infty} W(x, y)dxdy = 1 \tag{A4}$$

3. To satisfy the basic requirement (2.7), there must be:

$$\int_{-\infty}^{+\infty} W(x, y)dx = g(y) \tag{A5}$$

Now, we want to find the $W_{\min}(x, y)$ which minimizes "disturbance" to the sequence, quantified as

$$B[W] = \int_{-\infty}^{+\infty} (x - y)^2 W(x, y)dxdy$$

We want to show that the distribution $W_{\min}$ must be zero almost everywhere on the xy plane. Suppose we have found such a $W_{\min}$, and $W_{\min}(x, y) > 0$ everywhere in a small region $\mathcal{A}$. We can always find some function $S_{\mathcal{A}}(x, y)$ which is nonzero only inside $\mathcal{A}$ and satisfies

$$\int_{\mathcal{A}} S_{\mathcal{A}}(x,y)dx = 0 \tag{A6}$$

$$\int_{\mathcal{A}} S_{\mathcal{A}}(x,y)dy = 0 \tag{A7}$$

For instance in a rectangular area $(x_1, y_1) - (x_2, y_2)$ we can pick $S_{\mathcal{A}}$ to be

$$S_{\mathcal{A}}(x,y) = \sin(2\pi n_x \frac{x - x_1}{x_2 - x_1}) \sin(2\pi n_y \frac{y - y_1}{y_2 - y_1}) \tag{A8}$$

where n_x, n_y are non-zero integers, and zero elsewhere. Since the expression for $B[W]$ contains $(x-y)^2$, it can not be that

$$B[S_{\mathcal{A}}] = 0 \tag{A9}$$

for all valid $S_{\mathcal{A}}$'s, and we can always choose a small enough λ to ensure that $|\lambda S_{\mathcal{A}}(x,y)| \leq W(x,y)$ everywhere. Let

$$W_{\text{new}} = W_{\min} + \lambda S_{\mathcal{A}} \tag{A10}$$

W_{new} will also satisfy the constraints (A2) to (A5). Lastly let us pick the sign of λ to make $\lambda B[S_{\mathcal{A}}] < 0$, so

$$B[W_{\text{new}}] = B[W_{\min}] + \lambda B[S_{\mathcal{A}}] < B[W_{\min}] \tag{A11}$$

which is a contradiction. So, a finite area $\mathcal{A}$ where $W_{\min}(x,y) > 0$ does not exist, and $W_{\min}$ must equal to zero almost everywhere, which can only be satisfied if $W_{\min}(x,y)$ are combinations of δ-functions; that is, the optimal transformation $\mathcal{T}$ is a function-like mapping from X to Y, without any randomness.

Now, assuming $W_{\min}$ takes the form

$$W_{\min} \sim \delta(y - H(x)) \tag{A12}$$

which is equivalent to saying that the transformation is in fact a function $y = H(x)$. Then the problem simplifies to finding a function $H_{\min}$ which minimizes the sum (for illustrative purposes we use summation here instead of integration)

$$B[H] = \lim_{N\to\infty} \sum_i (x_i - H(x_i))^2/N \tag{A13}$$

with the requirement that x_i's are randomly drawn from distribution f and $H(x_i)$'s are randomly distributed with distribution g.

We want to show that $H_{\min}(x)$ must be a monotonically non-decreasing function: because if there exists a pair

$$x_1 > x_2 \;\text{ but }\; H(x_1) < H(x_2)$$

we can construct an $\tilde{H}(x)$ with x_1, x_2 exchanged

$$\tilde{H}(x) = \begin{cases} H(x) & (x \neq x_1, x \neq x_2) \\ H(x_2) & (x = x_1) \\ H(x_1) & (x = x_2) \end{cases} \tag{A14}$$

without influencing g, but

$$\begin{aligned}
&(x_1 - \tilde{H}(x_1))^2 + (x_2 - \tilde{H}(x_2))^2 \\
&= (x_1 - H(x_2))^2 + (x_2 - H(x_1))^2 \\
&= (x_1 - H(x_1))^2 + (x_2 - H(x_2))^2 \\
&\quad -(x_1 - x_2)(H(x_2) - H(x_1)) \\
&< (x_1 - H(x_1))^2 + (x_2 - H(x_2))^2
\end{aligned}$$

So $B[\tilde{H}] < B[H]$, which means $H_{\min}(x)$ must be a monotonically non-decreasing function.

Thus there is a unique, one-to-one relation between x and y, and there must be, because of (2.7),

$$dP = f(x)dx = g(y)dy \tag{A15}$$

because any small interval $(x, x + dx)$ is uniquely and deterministically mapped into $(y, y + dy)$ by the optimal transformation. So if we integrate from $x, y \to -\infty$ where $P = 0$, there must be

$$\int_{-\infty}^{x} f(\xi)d\xi = \int_{-\infty}^{y} g(\xi)d\xi$$

which is the $\mathcal{T}_3$ transformation of (2.10).

---

[1] J. Koplik, J. R. Banavar, Annu. Rev. Fluid Mech. **27** 257 (1995).

[2] S. T. O'Connell and P. A. Thompson, Phys. Rev. E **52**, 5792 (1995).

[3] N. Hadjiconstantinou and A. T. Patera, *International Journal of Modern Physics* C **8** 967, (1997).

[4] J. Li, D. Liao and S. Yip, Phys. Rev. E **57**, 7259 (1998).

[5] P. L. Lions, in *First International Symposium on Domain Decomposition Methods for Partial Differential Equations*, 1-42, SIAM 1988; J. F. Bourgat *et al*, in *Fifth International Symposium on Domain Decomposition Methods for Partial Differential Equations*, 420-440, SIAM 1991.

[6] B. F. Smith, P. E. Bjorstad, W. D. Gropp, *Domain Decomposition: Parallel Multilevel Methods for Elliptic Partial Differential Equations* (Cambridge University Press, 1996).

[7] See for instance, A. L. Greensite, *Control Theory* (Spartan Books, 1970).

[8] P. A. Thompson and M. O. Robins, Phys. Rev. A **41**, 6830 (1990).

[9] See for instance, R. Phillips, JOM. **47** 37 (1995); E. B. Tadmor, M. Ortiz, R. Phillips, Phil. Mag. A**73** 1529 (1996).

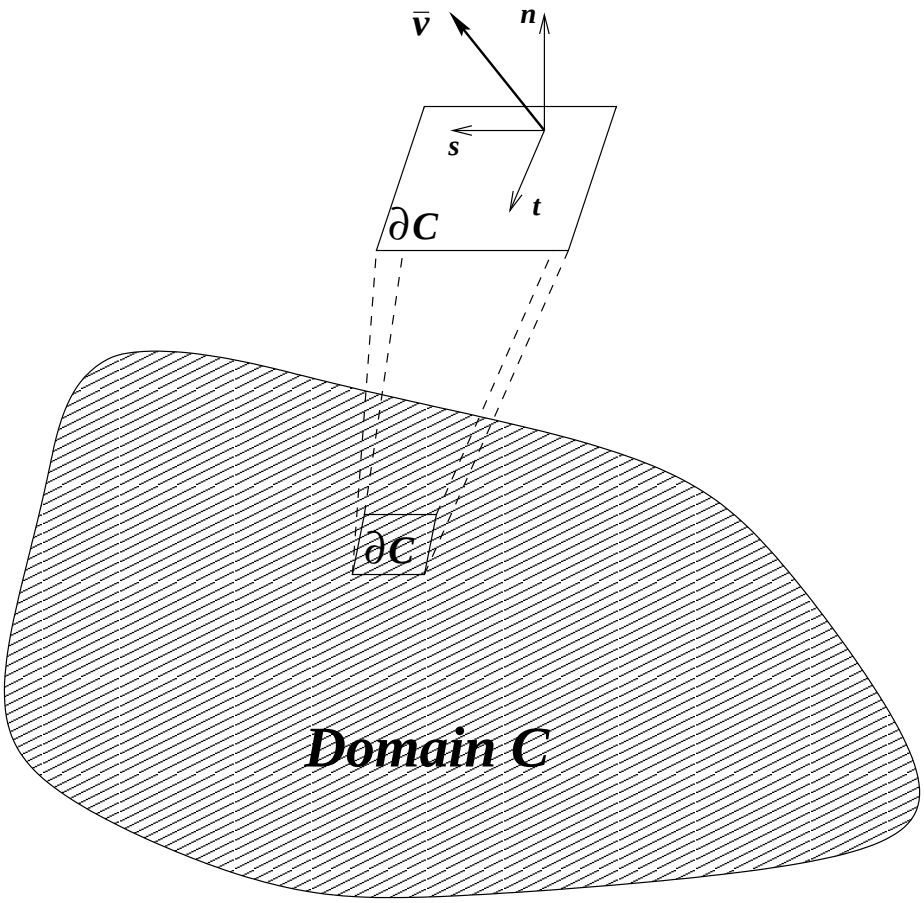

FIG. 1. In the direct approach, $\mathcal{C}$ is our domain of interest, $\partial\mathcal{C}$ is its boundary which the particle controller acts on to achieve the desired macroscopic fields. For any small piece of the boundary, we choose the local coordinate frame to express the prescribed macroscopic velocity field as $\bar{\mathbf{v}} = (v_n, v_s, 0)$. In the same frame the actual, or current velocity field is $\bar{\mathbf{v}}' = (v_n', v_s', v_t')$.

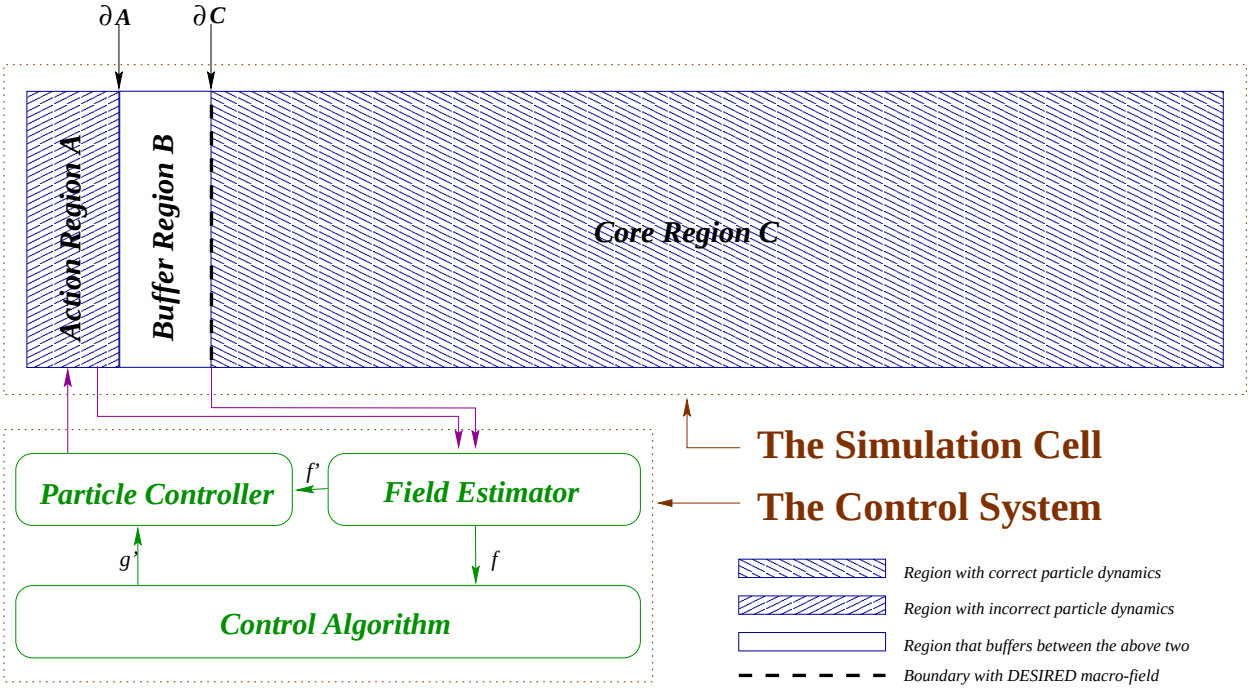

FIG. 2. Schematic diagram of the Extended Boundary Condition (EBC), which incorporates a field estimator, a particle controller and a feedback control algorithm.

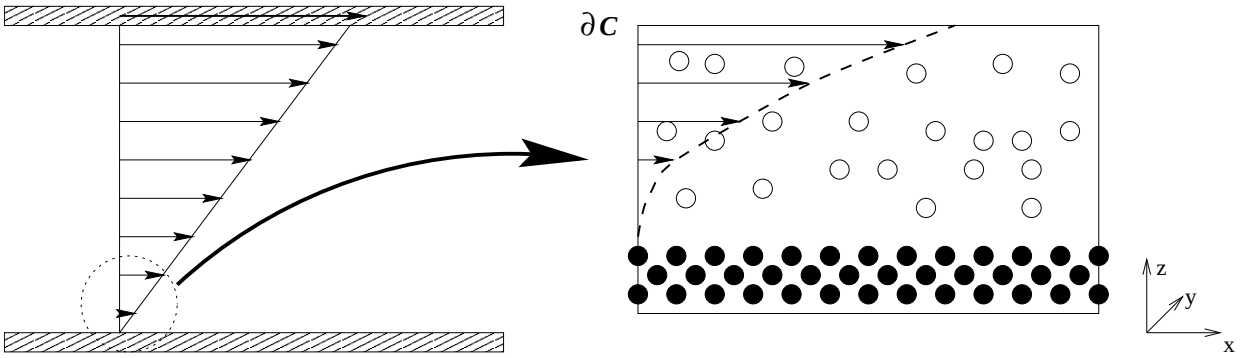

FIG. 3. Geometry for simulation of planar Couette flow. The continuum solution is a linear velocity profile, $\bar{v}_x(z)$. In the atomistic description, the fluid is represented by N particles evolving according to molecular dynamics, and the wall is modeled by three layers of stationary particles which interact with the fluid. Dashed line depicts qualitatively the expected flow velocity profile on the molecular scale.

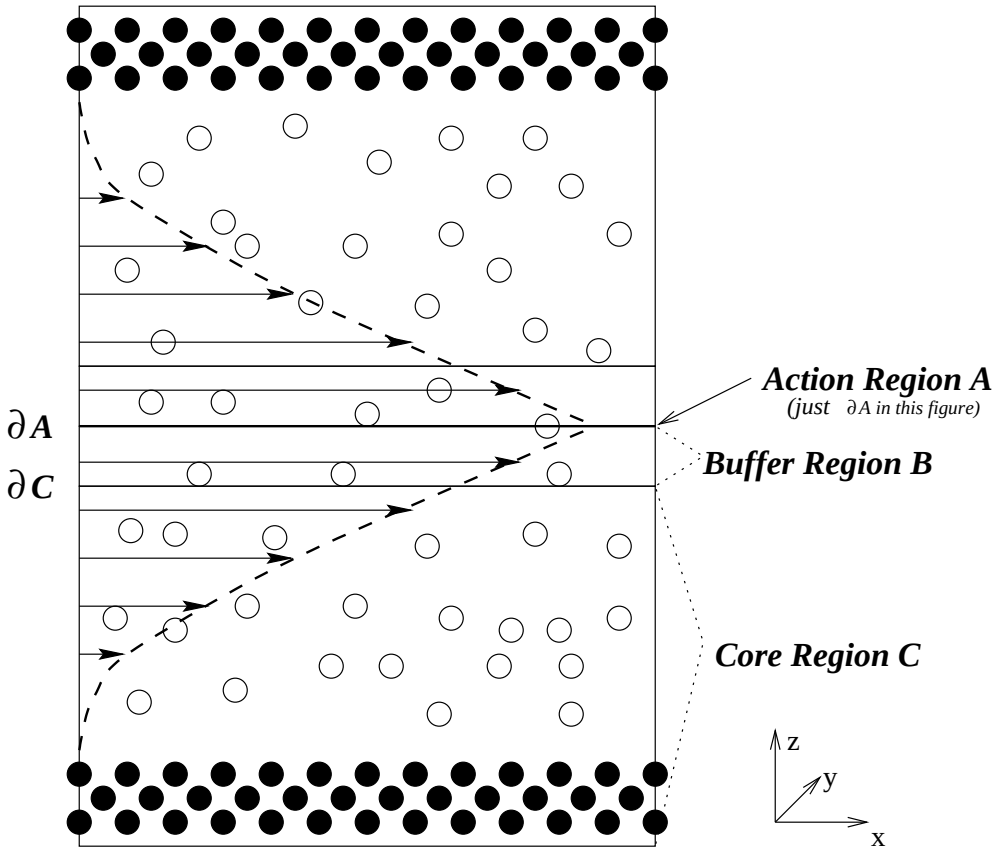

FIG. 4. MD simulation cell incorporating the Extended Boundary Condition (EBC). A buffer region $\mathcal{B}$ (between $\partial\mathcal{A}$ and $\partial\mathcal{C}$) is inserted between the physical region of interest $\mathcal{C}$ and the action region $\mathcal{A}$ (just a plane $\partial\mathcal{A}$). The simulation cell is symmetric with respect to $\partial\mathcal{A}$.

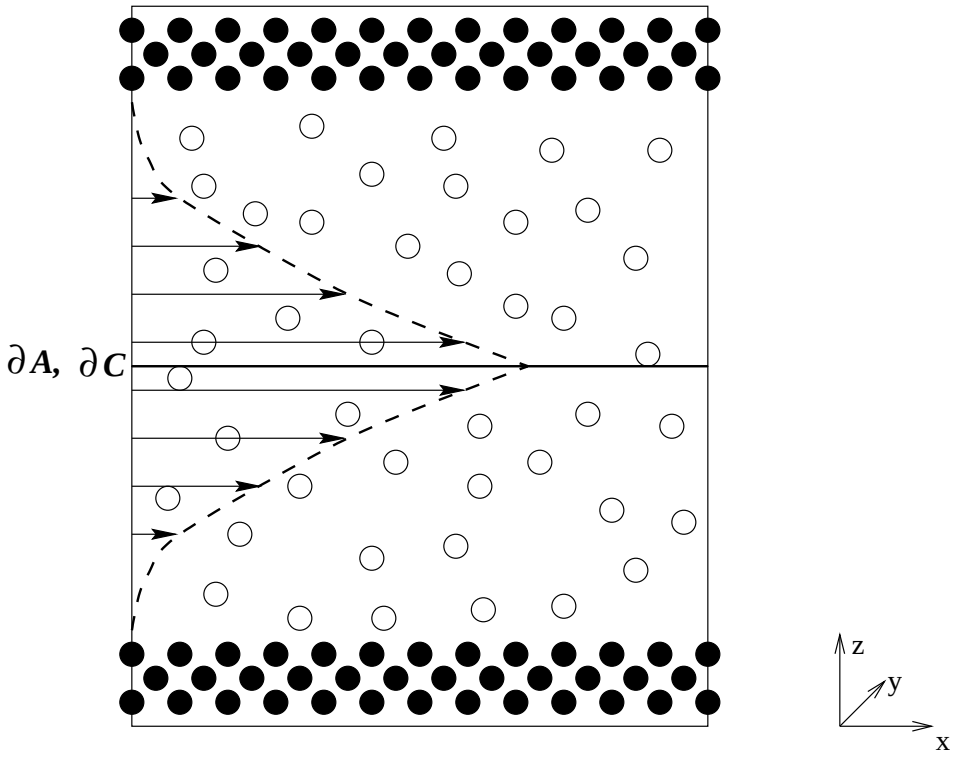

FIG. 5. Direct particle controller boundary condition, where ∂A and ∂C are brought together and there is no buffer.

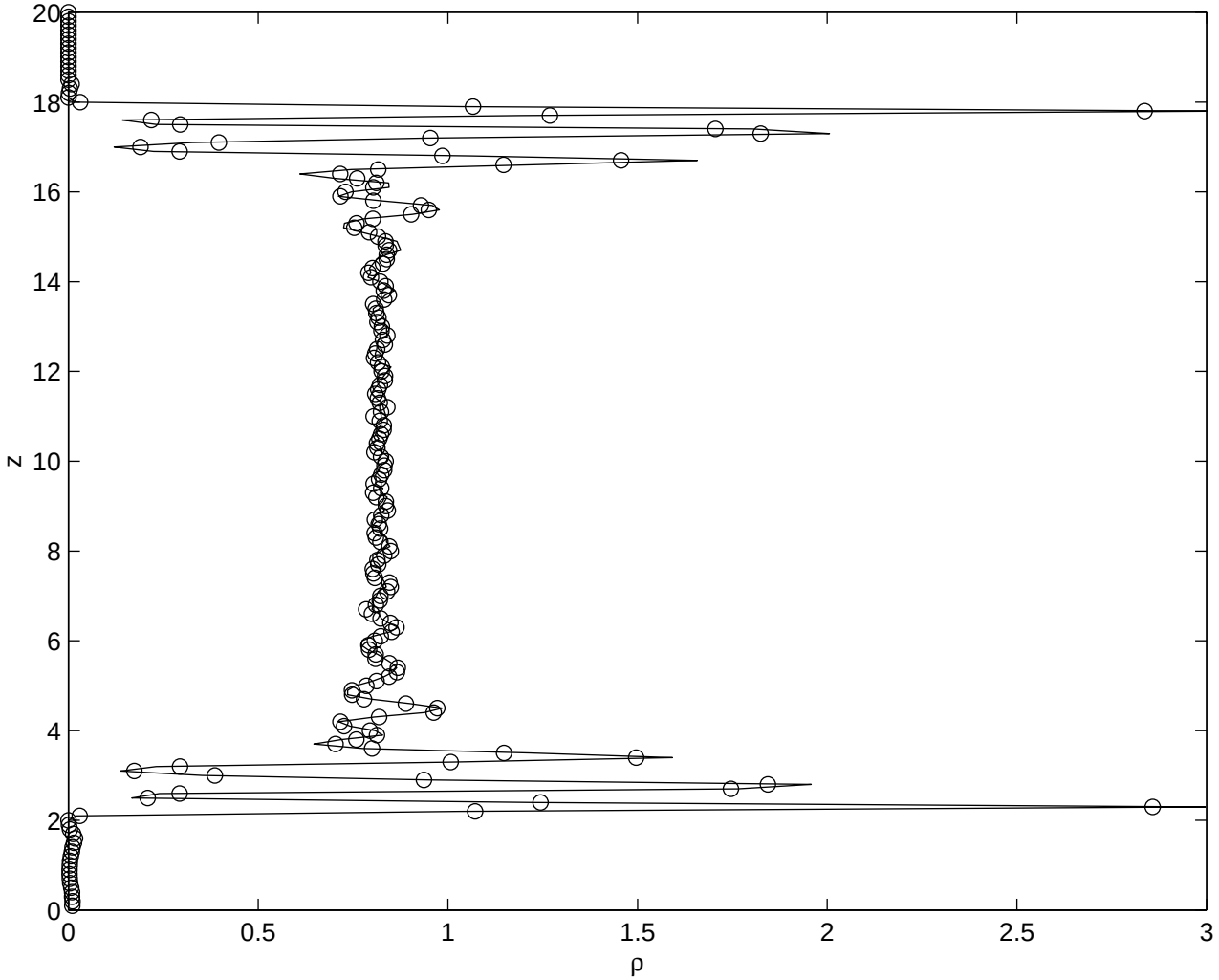

FIG. 6. Density profile of the fluid in the simulation cell with (circles) and without (solid line) shear flow. The solid wall end at $z = 2$ and $z = 18$.

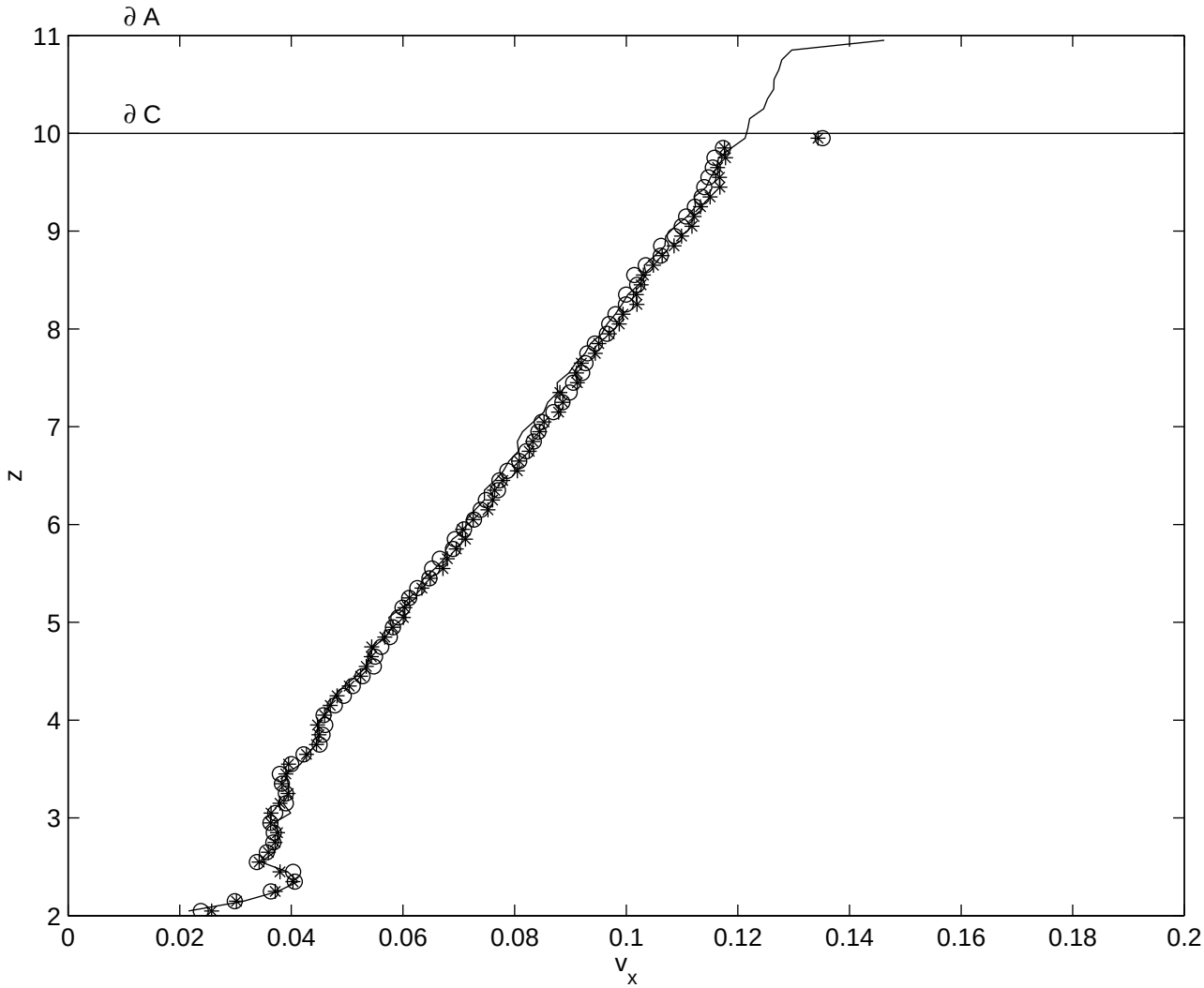

FIG. 7. Profile of shear flow velocity $\bar{v}_x(z)$ obtained from three different MD simulations: smooth line is result from EBC (Fig. 4); stars and circles are results from direct particle controller simulations (Fig. 5) using $\mathcal{T}_1$ and OPC.

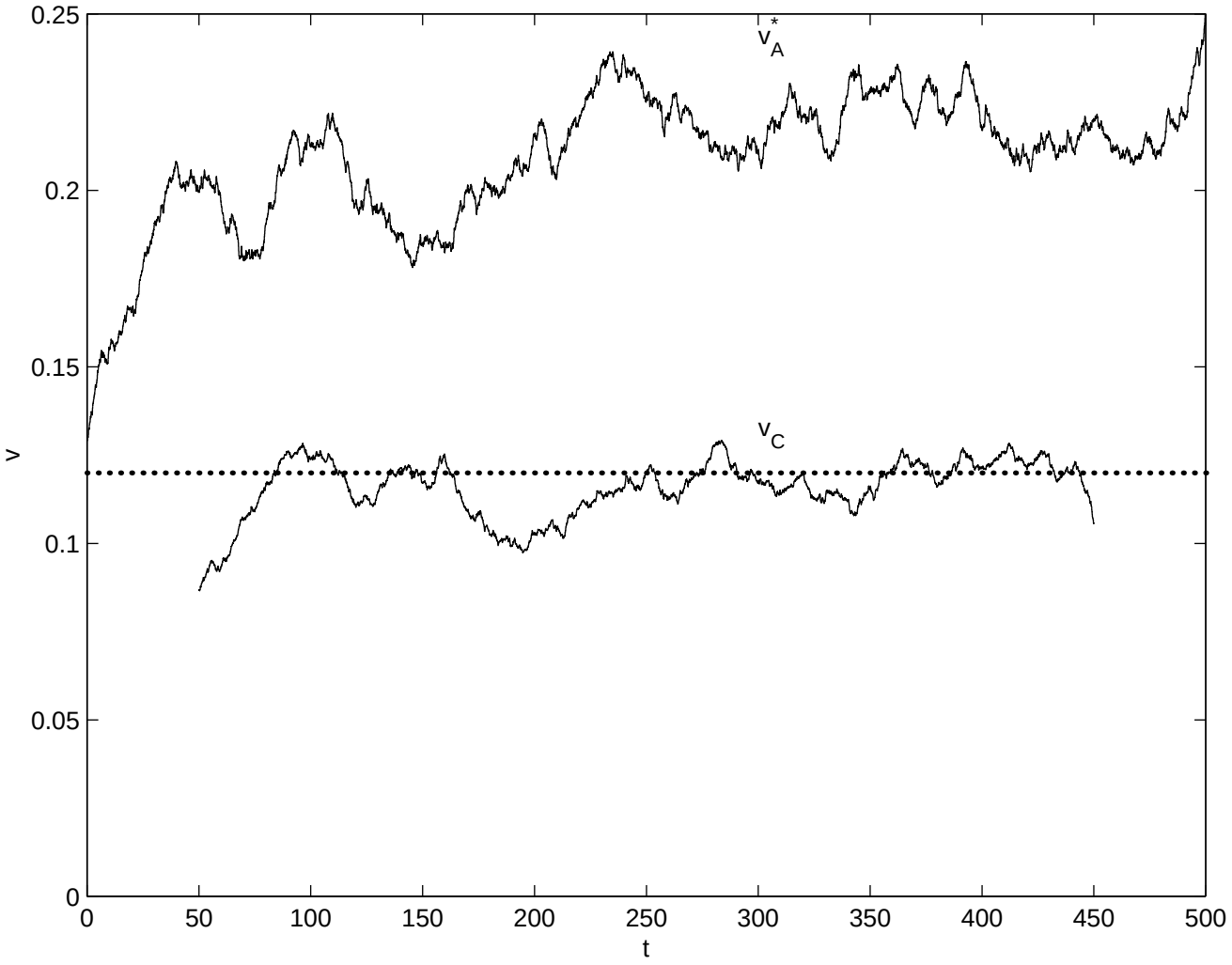

FIG. 8. Starting with zero flow velocity $v_C(0) = 0$ and the prescribed velocity $v_A^*(0) = 0.12$, this plot shows how v_A^* and v_C evolves in time. $v_C(t)$ in this graph is the sliding bin average over $\Delta t = 50\tau$. For comparison, v_C^* is plotted in dotted line. Convergence in both v_C and v_A^* is obtained at around $t = 80$.

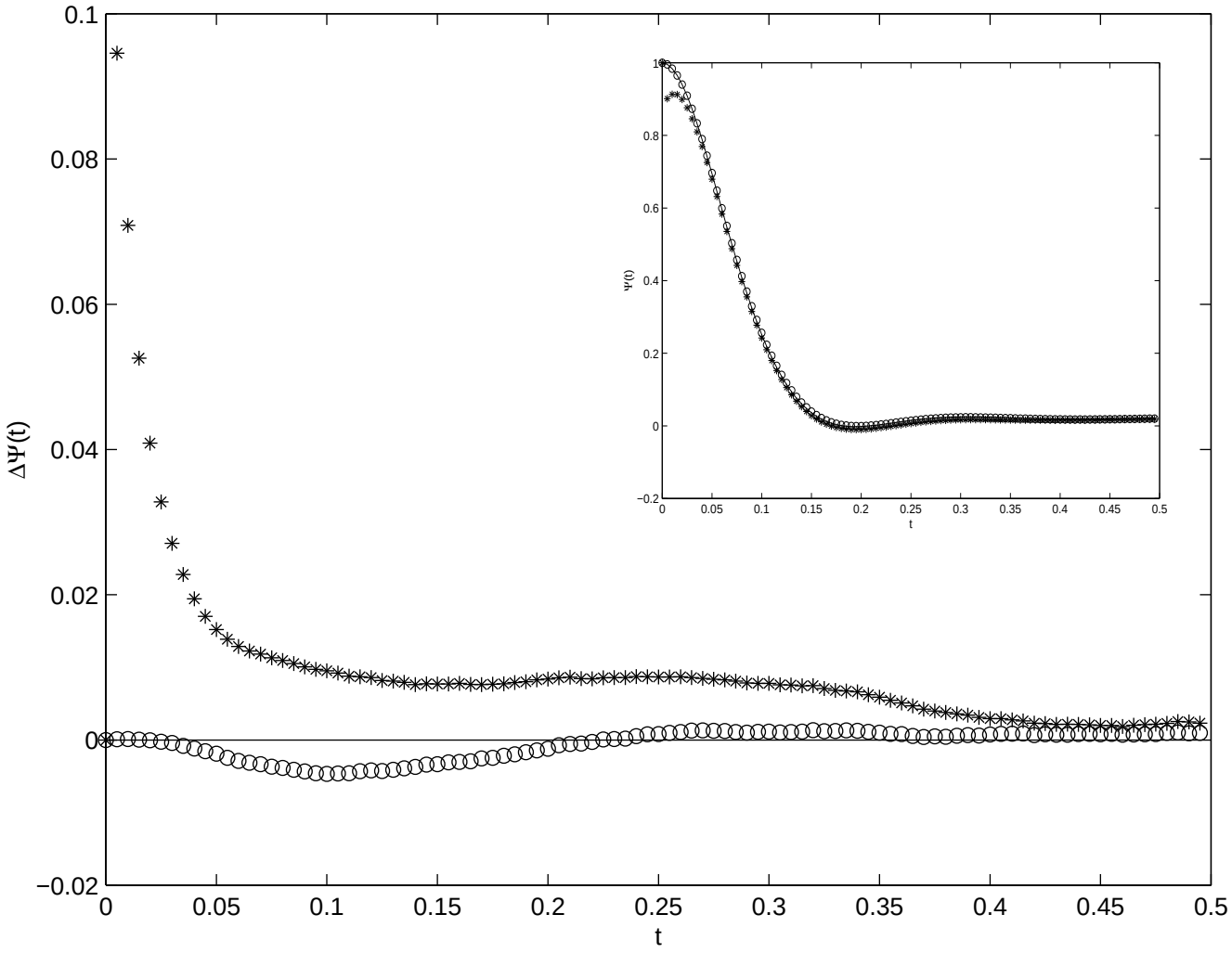

FIG. 9. Comparison of the change to the normalized velocity autocorrelation function $\Psi(t)$ due to $\mathcal{T}_1$ and OPC. $\Psi_{\rm EBC}(t) - \Psi_{\mathcal{T}_1}(t)$ is plotted in stars and $\Psi_{\rm EBC}(t) - \Psi_{\rm OPC}(t)$ is plotted in circles. In the inset, $\Psi_{\rm EBC}(t)$, $\Psi_{\mathcal{T}_1}(t)$ and $\Psi_{\rm OPC}(t)$ are plotted in solid line, stars and circles respectively. Notice that $\Psi_{\mathcal{T}_1}(0) = 1$, but it is quickly scattered in the ensuing period.

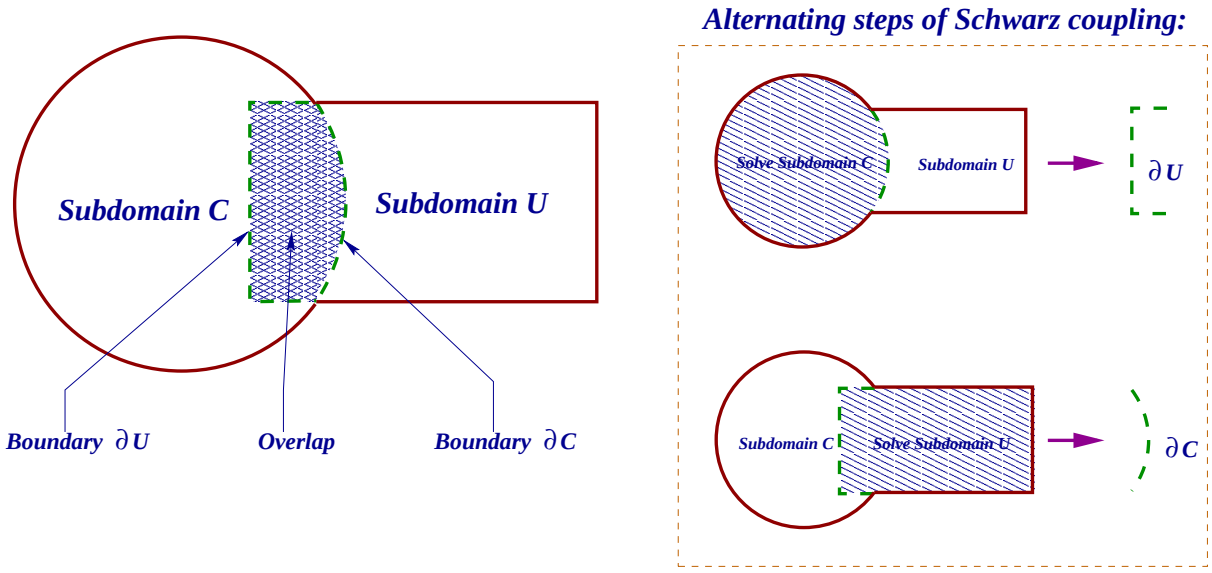

FIG. 10. Classical alternating Schwarz method, which joins the two overlapping regions/solvers $\mathcal{C}$ and $\mathcal{U}$ through iteration of boundary conditions.

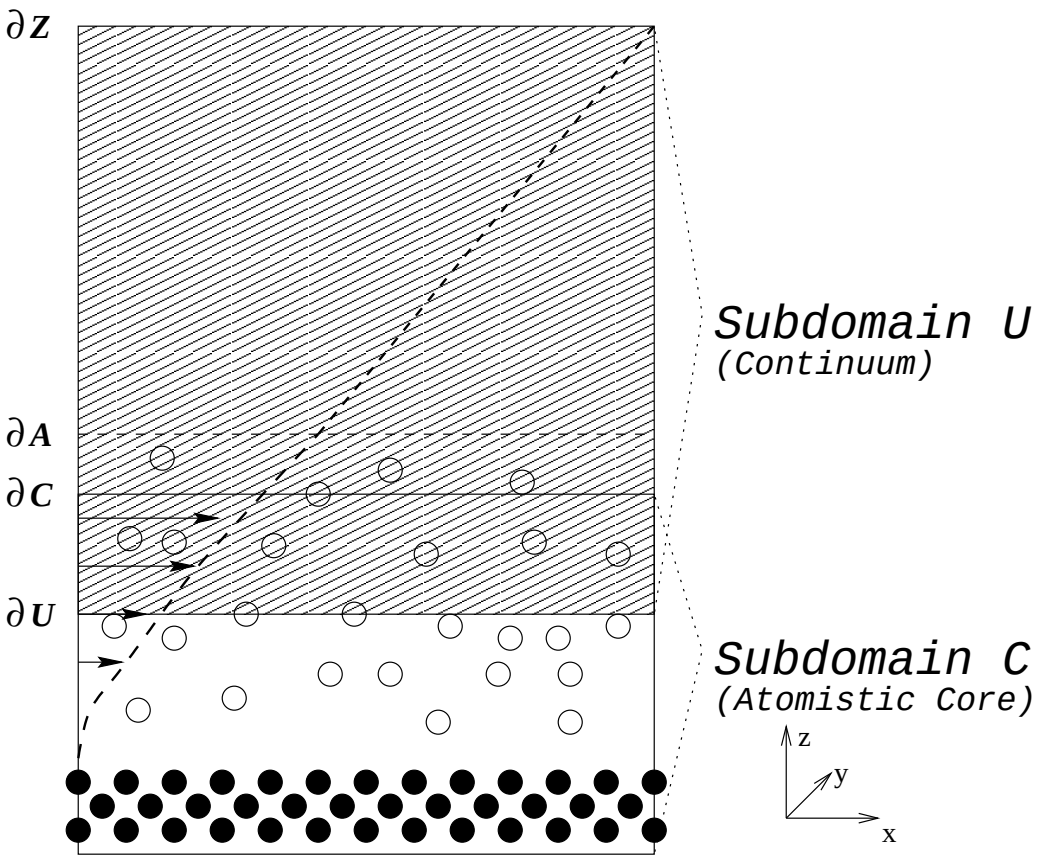

FIG. 11. Geometry of Schwarz coupling in simulating shear flow.

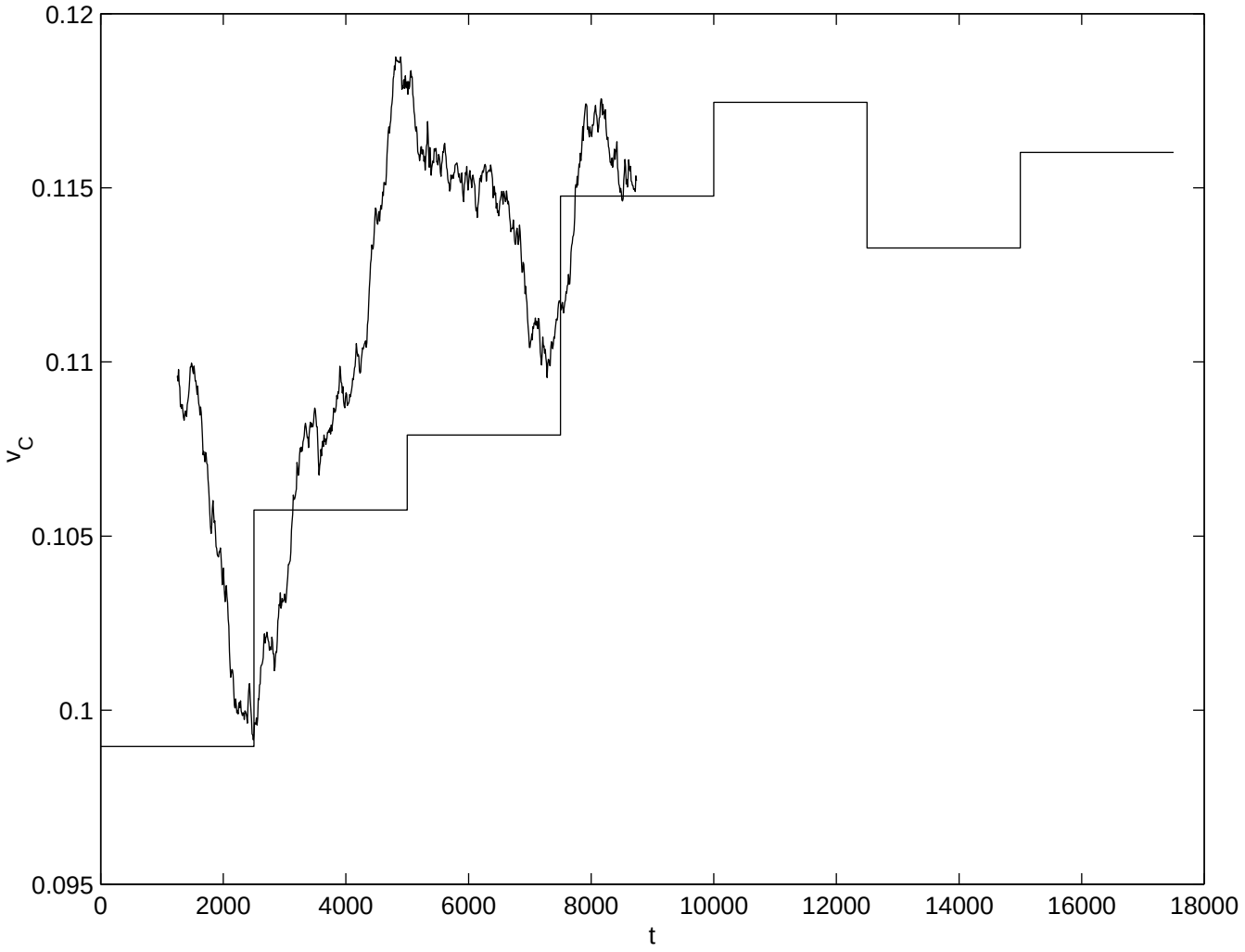

FIG. 12. Comparison of convergence speed using classical alternating Schwarz method (straight lines), and the simultaneous relaxation method (zigzag lines) which takes advantage of the fact that the continuum solver takes no time at all for this simple scenario.

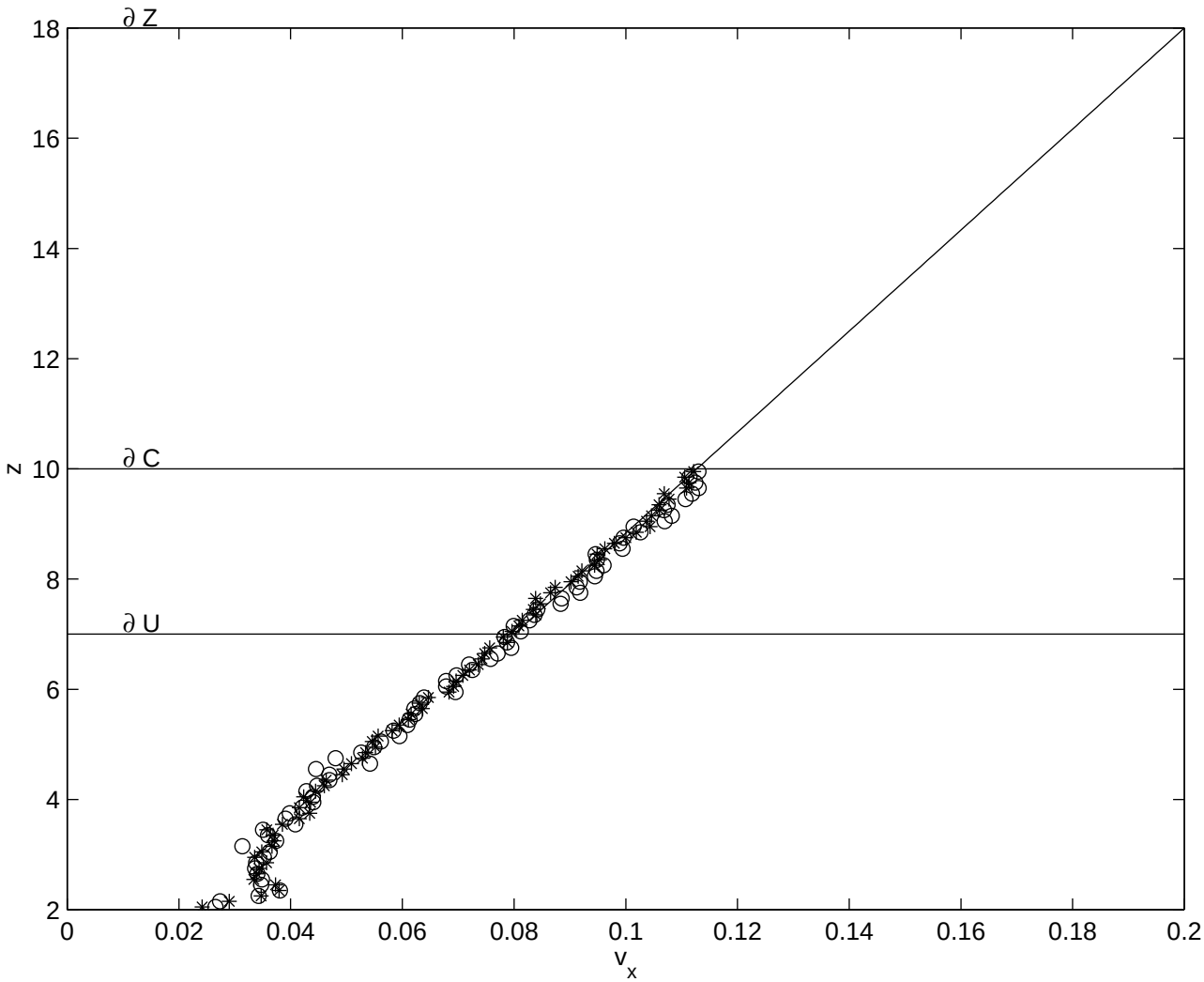

FIG. 13. Fully converged hybrid continuum-atomistic solution. The classical alternating Schwarz method (circles) and the simultaneous relaxation method (stars) give essentially the same result, and there is good matching with the continuum solutions in the overlapping region.